

Development of silica - cenosphere aerogel composites for thermal insulation applications

R. Manikandan, D. Thenmuhil*, M. Krishnan

Department of Ceramic Technology, Alagappa College of Technology Campus, Anna University, Chennai - 600 025, Tamil Nadu, India

Novel aerogel composites were prepared by sol-gel process and dried by adding 5 to 15 weight percentage of cenosphere to silica aerogel prepared by subcritical drying process. Silica-cenosphere aerogels were calcined at 1200°C, as α -cristobalite phase was formed in silica aerogel at 1200°C. At temperatures less than 1200°C only amorphous silica was found in silica aerogel. Microstructural analysis showed spherical shape in different sizes with micro pores in surface of cenosphere and popcorn-like structure in silica-cenosphere aerogels. Effect of cenosphere addition in silica aerogel was studied by FT-IR. The particle size and distribution of prepared aerogels and cenosphere were analysed by particle size distribution analyser. The average particle size of silica aerogel was found to reduce by increased addition of cenosphere. The nitrogen adsorption studies of cenosphere and silica-cenosphere aerogels indicated type II isotherm which represents macroporous/nonporous unrestricted monolayer – multilayer adsorption. The powder flow behaviour of the cenosphere and prepared aerogels were found to be strongly dependent on the particle size and distribution. The compressive strength and thermal conductivity of all the samples were found to be dependent on the porosity and bulk density. Among all the samples, lower density and higher porosity was observed in SC15. The silica aerogel recorded the highest strength value and was reduced by the addition of cenosphere except for SC5. The thermal conductivity was also found to be lowered for silica-cenosphere aerogels than pure silica aerogel and was found suitable for thermal insulation application that do not require strength.

(Received October 9, 2023; Accepted January 10, 2024)

Keywords: Aerogel, Subcritical drying, Silica-cenosphere, Thermal conductivity, Thermal insulation, Composites

1. Introduction

Aerogels are stable, open-celled, mesoporous foams with a porosity of at least 50% and are made up of a network of interconnecting nanostructures [3]. Typically, sol-gel synthesis followed by novel drying techniques are used to create aerogels from a large variety of chemical precursors [2]. One of the most widespread procedures used to create silica gels is the alkoxide gelation, which involves the polymerization of silicon alkoxide on reaction with water in the presence of a basic catalyst, often in ethanol or acetone medium. The silicon alkoxides commonly used are tetramethylorthosilicate (TMOS) or tetraethyl orthosilicate (TEOS). A fundamental catalyst that speeds up the polymerization process is ammonium hydroxide. Generally, three drying methods for gels can be distinguished as below.

(1) Traditional hot air-drying that results in creation of xerogel. Significant shrinkage during drying makes it difficult to maintain the gel structure. (2) Freeze-drying process which involves lowering the temperature of the gel below the solvent's crystallisation point while the solvent is evacuated as a vapour by reducing the pressure. The end product of this approach is typically referred to as cryogel. This process is expensive and unsuitable for large-scale manufacturing. (3) Supercritical drying involving supercritical fluids like CO₂ that helps to overcome the problems with conventional drying processes [2]. Aerogels produced under supercritical drying conditions

* Corresponding author: thenmuhil@annauniv.edu
<https://doi.org/10.15251/DJNB.2024.191.81>

have very low densities and significant porosities [6]. Many oxide aerogels are now made by supercritical drying, but this process is energy-intensive, risky, and expensive.

For the manufacture of oxide aerogels, the subcritical drying approach, also known as ambient pressure drying (APD), is essentially more straightforward and practical than the supercritical drying method. This technique can produce aerogels economically on a large scale and involves less risk [3]. It is another approach to minimise the cost and energy used to produce aerogels and depend upon substitution of organic low-surface tension solvents, such as hexane, heptane, octane, etc. for the original solvents used for gel formation [28]. X.han et.al. [29] created a new APD technique approach. Instead of surface modification and solvent exchange, they used a mixture of sodium bicarbonate solution and TMCS to treat the wet gel. CO₂ was formed inside the wet silica gel without surface modification, and the creation of a bubble of CO₂ gas in a gel pore opposes capillary pressure.

Here, the gel was soaked in a succession of stock solutions for ageing and the solvent was exchanged. The gel was then dried in air and fired at a proper temperature [6]. This method frequently results in fragile gels, and when the lack of pore liquid during drying was corrected, the solvent extraction under air tension causes lateral compressive strain in the gel [1]. By reducing the capillary force and also by enhancing the gel network's stiffness, the ensuing shrinkage could be minimised. This was accomplished by introducing sodium silicate or TEOS into the gel network to strengthen it [6]. In the current work, cenosphere was added as reinforcement in the silica gel network resulting in formation of silica-cenosphere aerogel composites

A cross-linked internal structure of silica that contains many air-filled nano-scale pores is known as silica aerogel. At present, silica aerogel is recognised globally as one of the most attractive thermal insulating materials for usage in aircraft, building constructions, and other applications [24]. Silica aerogels are attracting much attention due to their highly low density, relatively low thermal conductivity, and enormous specific surface area [10,11]. These outstanding characteristics lead to applications in various fields, notably thermal insulation [12-14, 26], separation of the oil from the water [15] and removing an oil-spill [16-19], supports for catalyst [20-21], aerospace applications [22-23], thermal and acoustic insulators, catalytic converters, carriers of active substances, absorbents of gases, liquids and sensors [25], drug delivery and humidity sensor [26]. Silica aerogels are employed in ceramic-ceramic composites, as materials with low dielectric constants (silica aerogel films), in clothing as apparel and blankets and templates [27]. However, as silica aerogel sinter at temperatures above 600°C, it has limited thermal pore stability making it unsuitable as high temperature insulation material [6].

Cenospheres are light weight, thin-walled hollow microspheres that are mostly composed of alumina and silica, are thermally stable, and are filled with air or inert gas. They are typically handled as waste by-products of thermal power plants that uses coal as fuel. Due to its distinctive characteristics, cenospheres are utilised in a variety of industries. These characteristics include their spherical shape, hollow interior, low specific gravity, low thermal conductivity, high strength, and resistance to acids and alkalis. Because of their hollow, micro-spherical structure and low density, cenospheres are commonly employed as a filler to reduce the density of materials like ceramics and polymers [5]. Reinforcement of the cenosphere creates closed pores and reduces weight.

Several engineering applications, among them including energy, construction, aeronautics and astronautics, impose significant importance on insulation materials. One of the most significant variables that reveals the insulation efficacy of the material used for thermal insulation is thermal conductivity. Super thermal insulation material is silica aerogel with low thermal conductivity [26].

In this present work, silica-cenosphere aerogels with different weight percentages of cenosphere were prepared. Cenospheres were added during silica aerogel preparation by sol-gel process which was subsequently subjected to subcritical drying.

2. Experimental details

2.1. Reagents

The chemicals used for silica aerogel synthesis were tetraethyl orthosilicate, formally named tetraethoxysilane (TEOS, 98%), Trimethylchlorosilane (TMCS, 98%), Ammonium hydroxide

(Ammonia) solution (25%), n-Hexane (99% purity), Ethanol and Acetone. Cenosphere of CIL 120 grade was purchased from Cenosphere India Pvt. Ltd., Kolkata. Cenospheres were used in as-received condition without any surface or heat treatment. Deionized water was used for all the experiments. All chemicals were used as received without any further treatment or processing.

2.2. Experimental work

The silica aerogel was prepared following the procedure described by Tomasz Blaszczyński et.al. [4]. The silica aerogel was synthesized using TEOS with ammonium hydroxide, deionized water and ethanol by sol-gel process. The obtained silica gel was aged for 24 hours in acetone and was subsequently subjected to subcritical drying which was critical for the stability of silica aerogel. In this process, the stock solutions were prepared [3] using low surface tension solvents such as hexane, ethanol or methanol, TMCS and deionized water and soaked in each solution for 24 hours. Then this gel was dried at room temperature and fired at different temperatures such as 600°C, 800°C, 1000°C and 1200°C to obtain powdered silica aerogel. To prepare silica-cenosphere aerogels, cenosphere was added in different weight percentages such as 5wt%, 10wt% and 15wt% to the silica precursor solution during sol-gel synthesis. Subsequent procedures were followed similar to preparation of silica aerogel. The obtained samples were dried in atmospheric condition and fired at 1200°C since silica aerogel was found to become crystalline at that temperature. The resultant samples were labelled SC5, SC10 and SC15 based on the weight percentage of cenosphere added. 13mm diameter pellets of the cenosphere and aerogel samples were prepared by uniaxial pressing with applied pressure range of 500 kg/cm². Chemical characteristics, phase analysis, microstructure identification, and confirmation of production material by FT-IR analysis, particle size distribution, and surface area analysis were carried out to characterise all of the produced aerogel powders. Measured physical attributes for powder includes tap density and flow character for the powder. The pellets are characterized for their bulk density, apparent porosity, water absorption, compressive strength and thermal conductivity.

The elemental composition of cenosphere and aerogels calcined at 1200°C was recorded using PANalytical range of XRF analyzer (AXIOS^{max} WDXRF). The XRD patterns were recorded with D8 advance (Bruker) using CuK α radiation ($\lambda=0.15406$ nm). The morphology study of prepared samples was investigated by High Resolution Scanning Electron Microscope (HR SEM F E I Quanta FEG 200). Fourier transform Infrared (FT-IR) spectra were taken in ATR-IR spectrometer. The specific surface area, pore volume and pore diameter values of silica-cenosphere aerogels were recorded after degassing in vacuum at room temperature for 2hr, using micromeritics ASAP 2020 porosimeter by nitrogen adsorption technique at liquid nitrogen temperature. The Practica Laser Scattering Particle Size Distribution analyser (LA-950V2) was used to determine the particle size and size distributions of prepared samples. Universal Testing Machine (UTM – HOUNSFIELD 50KN) was used to find out compressive strength of prepared samples. Thermal conductivity was measured by using LFA 467 HyperFlash apparatus. The bulk density (BD), apparent porosity (AP) and water absorption (WA), values were calculated using Archimedes' principle.

$$\text{Bulk density (g/cm}^3\text{)} = D / (W-S) \times 100 \quad (1)$$

$$\text{Apparent porosity (AP \%)} = [(W- D) / (W-S)] \times 100 \quad (2)$$

$$\text{Water absorption (WA\%)} = [(W-D) / D] \times 100 \quad (3)$$

where, dry weight (D), soaked weight (W), and suspended weight (S)

The true/tap density values of powder samples were calculated using the graduated cylinder method. Using the Hausner ratio (HR) and the compressibility index, also known as Carr's Index (CI), flowability of prepared samples were assessed. Equations 4 and 5 were used to determine HR and CI respectively [7, 8].

$$\text{Hausner Ratio (HR)} = \rho_t / \rho_b \quad (4)$$

$$\text{Compressibility Index (CI \%)} = [(\rho_t - \rho_b)/\rho_t] \times 100 \quad (5)$$

where, ρ_b is the bulk density in g/cm^3 and ρ_t is the true/ tap density in g/cm^3 of prepared aerogel samples.

3. Results and discussion

Table 1 displays the results of elemental compositions of the cenosphere, silica aerogel and silica-cenosphere aerogels involved in this study. The findings showed that the two main constituents of all the materials were alumina and silica. The prepared silica aerogel material principally contains silica (SiO_2), which accounts for 97.4% of its composition. Silica content was found to reduce with increase in addition of cenosphere. Although compositions are slightly different, there are no significant modifications. The silica-cenosphere aerogels also contains other components like K_2O , Fe_2O_3 , and TiO_2 as major impurities.

Table 1. Elemental Compositions.

Material	Weight %									
	SiO_2	Al_2O_3	CaO	Fe_2O_3	K_2O	MgO	Na_2O	P_2O_5	TiO_2	ZrO_2
Cenosphere	58.0	31.11	0.81	3.36	3.03	0.73	0.15	0.37	1.37	0.004
Silica Aerogel	97.4	1.51	0.04	0.10	-	0.05	0.01	0.003	0.02	0.06
SC5	94.2	4.33	0.12	0.48	0.49	0.13	0.002	0.04	0.18	0.07
SC10	92.6	5.04	0.15	0.59	0.55	0.18	0.003	0.05	0.19	0.07
SC15	92.2	5.61	0.16	0.66	0.57	0.17	0.006	0.06	0.25	0.05

Fig. 1 displays the diffraction patterns of silica-cenosphere aerogels as well as cenosphere and pure silica aerogels. In order to find the average crystallite size of the produced samples, the Debye Scherrer formula (Eqn. 6) was used.

$$D = 0.94\lambda/\beta\cos\theta \quad (6)$$

where D is the average crystallite size (in nm) λ is the radiation's wavelength (in nm), β is the corrected peak width at half maximum intensity (in radi.), and θ is the peak position (in deg.).

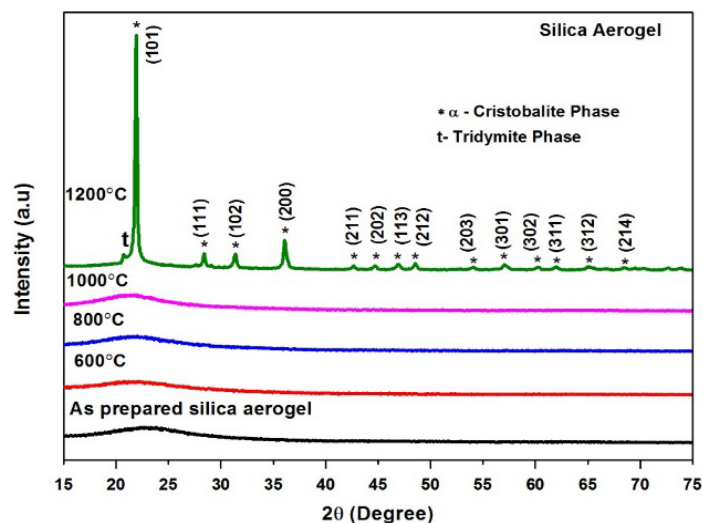


Fig. 1. XRD patterns of the silica aerogel calcined at different calcination temperatures

Fig. 1 displays the XRD pattern of pure silica aerogel samples heat treated at 600°C, 800°C, 1000°C, and 1200°C. The silica aerogel displayed pure amorphous silica phase pattern up to 1000°C. After being heated to 1200°C, amorphous silica crystallised into the principal tetragonal phase of α -cristobalite, with trace amount of tridymite phase. The highest and second-highest peaks, which were indexed at (101) and (200), were seen at 2θ of 21.985° and 36.08°, respectively. The additional peaks were indexed, and they matched JCPDS no. 39-1425. Formation of crystalline phase influences the thermal and mechanical properties of the silica aerogel. The average crystallite size of silica aerogel calcined at 1200°C was determined by Debye-Scherrer formula to be 24.38nm.

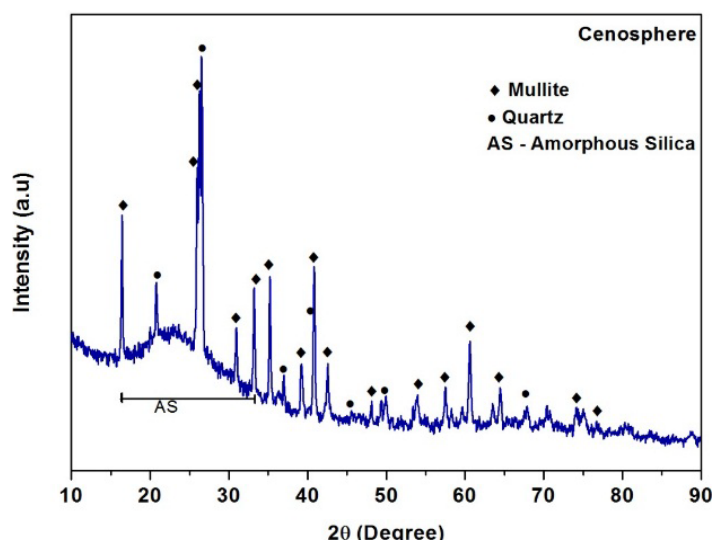


Fig. 2. XRD patterns of the cenosphere.

The XRD pattern of cenosphere sample is displayed in Fig. 2. Along with amorphous silica phase, the cenosphere contained the primary crystalline phases of quartz (SiO_2) and mullite ($\text{Al}_6\text{Si}_2\text{O}_{13}$). Wide bands in the 2θ range between 15 and 35° confirmed the amorphous silica phase. The phases of quartz and mullite matched JCPDS numbers 46-1045 and 15-0776, respectively. The mullite phase showed orthorhombic structure with primitive lattice and quartz phase showed hexagonal structure with primitive lattice. The crystallite size of cenosphere was found to be measured as 28.88 nm.

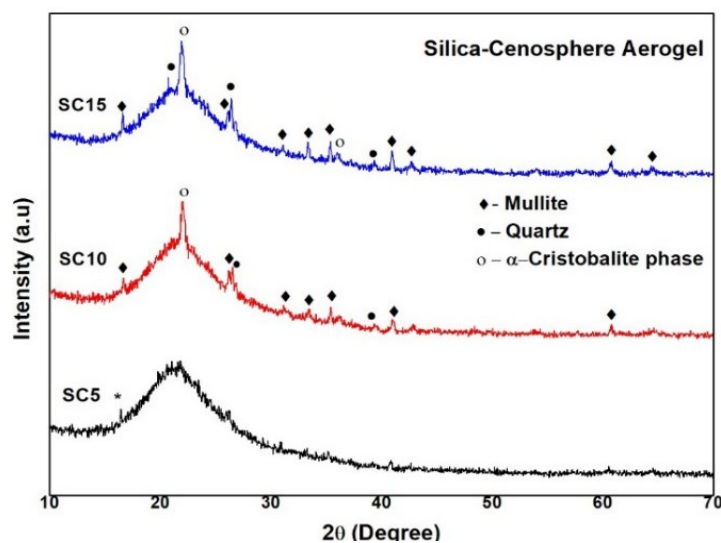


Fig. 3. XRD patterns of the silica – cenosphere aerogel composites.

Fig. 3 shows XRD patterns of Silica -cenosphere aerogels calcined at 1200°C. It shows completely mixed phases of mullite, quartz and α -cristobalite along with an amorphous silica phase. The intensities of amorphous silica in the silica-cenosphere composite aerogel were observed to be higher than that of cenosphere and the intensities of mullite, quartz and α -cristobalite phases were found to increase with increasing cenosphere content in silica aerogel. The amorphous phase of silica aerogel was found to be retained and its transformation into crystalline phase was retarded when adding cenosphere. The crystallite size was determined to be 1.92 μm , 0.356 μm , and 61.88 nm for SC5, SC10 and SC15 respectively.

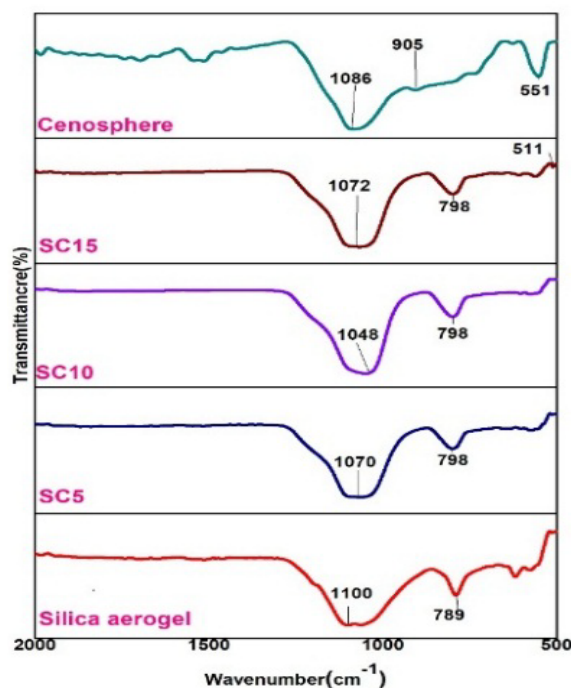


Fig. 4. FT-IR spectra of cenosphere, silica aerogel and silica- cenosphere aerogel composites calcined at temperature 1200°C

The FT-IR spectra of as-obtained cenosphere and that of silica aerogel and silica-cenosphere aerogels after being heat treated at 1200°C are shown in Fig. 4. The spectra shows that the cenosphere addition had no significant impact on SiO_2 polymerization. The peaks of cenosphere at 1086 cm^{-1} , 905 cm^{-1} , and 551 cm^{-1} are attributed to linear Si-O stretching vibrations in the Si-O-Si (SiO_2) system, strong Si-OH and Si-O-Si strains caused by the presence of the alumina and silicate phases, respectively. Si-O-Si stretching vibrations with strong absorptions are also responsible for the peaks in silica aerogel and silica-cenosphere composite aerogels at 1100 cm^{-1} , 1070 cm^{-1} , 1048 cm^{-1} , and 1072 cm^{-1} . Peaks at 789 cm^{-1} in silica aerogel and at 798 cm^{-1} in silica-cenosphere aerogels are attributable to Si-O symmetrical stretches. Due to the increased percentage of cenosphere content, the peak at 511 cm^{-1} in SC15 is attributed to the Si-O-Al asymmetrical bend stretch where Si-O-Al was formed due to substitutions of aluminium atoms for the silicon atom in Si-O-Si chain and this peak is not observed in SC5 and SC10.

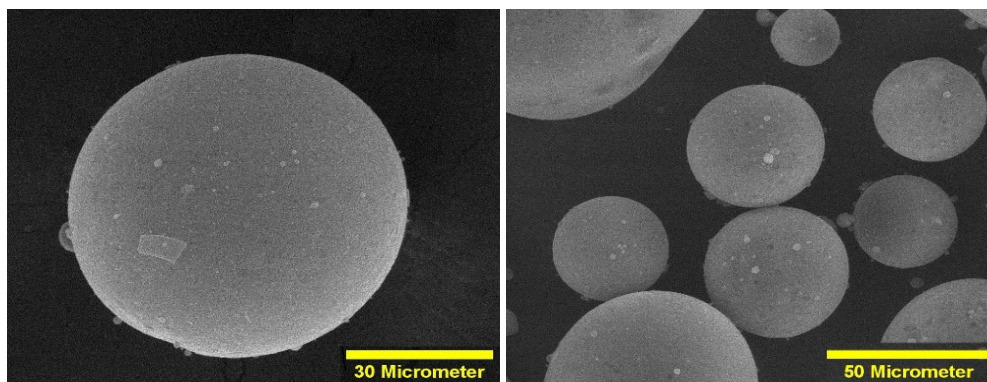


Fig. 5. HR-SEM images of Cenosphere at different magnifications.

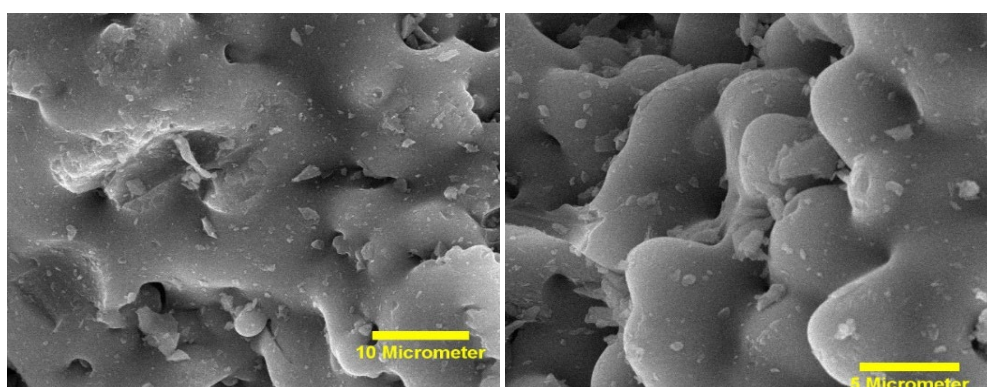


Fig. 6 HR-SEM images of Silica Aerogel at different magnifications

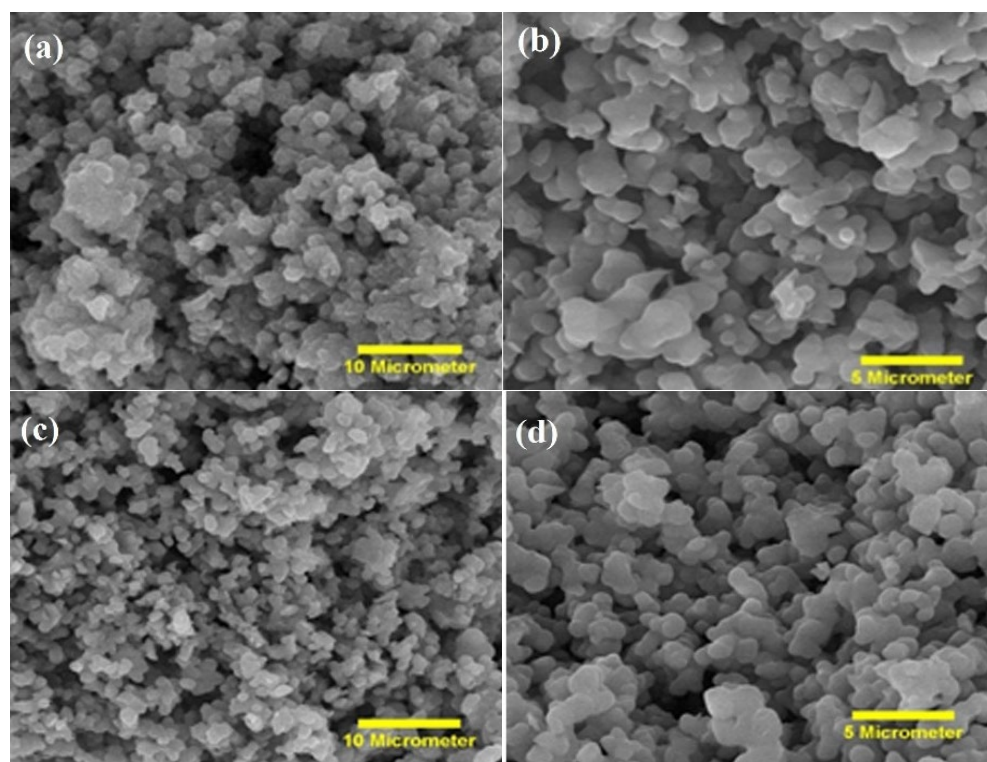


Fig. 7.1 HR-SEM images of (a) and (b) SC5, (c) and (d) SC10 at different magnifications.

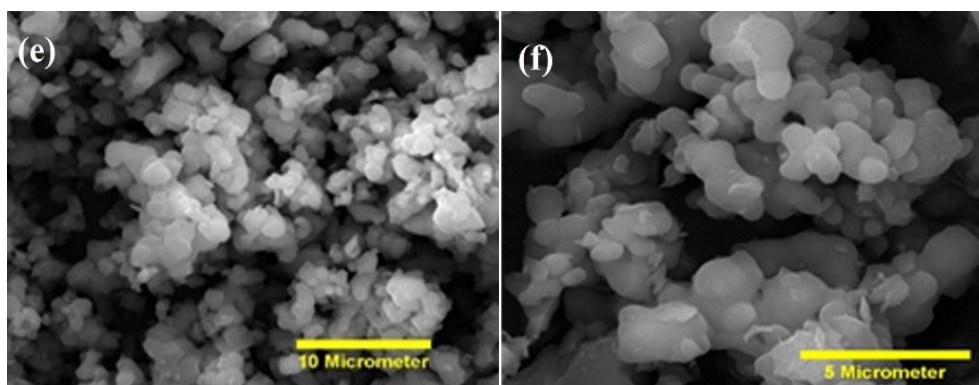


Fig. 7.2 HR-SEM images (e) and (f) SC15 at different magnifications.

Fig. 5, 6 and 7 shows the surface morphology of cenosphere, silica aerogel and silica-cenosphere aerogels at various magnifications.

Fig. 5 shows that cenosphere particles are predominantly spherical and come in a range of sizes. The surface of the cenosphere sample also exhibit micropores. A popcorn-like morphology can be detected in the HR-SEM pictures of silica aerogel sample after calcination at 1200°C in Fig. 6.

Fig. 7 displays the morphology of SC5, SC10, and SC15, respectively, at 10 μm and 5 μm magnifications. The morphology of SC5, SC10 and SC15 were almost identical to that of the silica aerogel and all the aerogel samples had popcorn -like particle morphology.

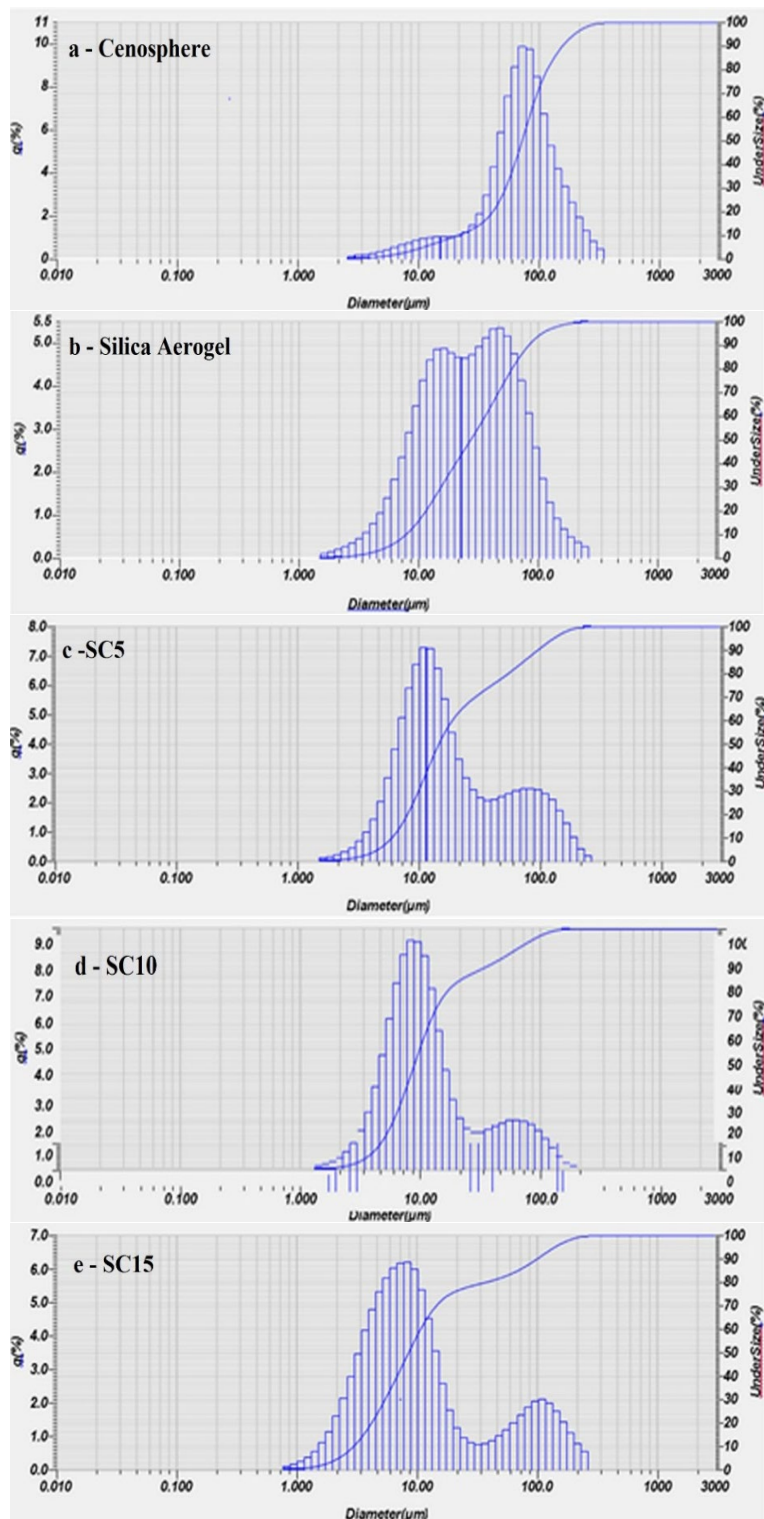


Fig. 8. Particle size and distributions curves of (a) Cenosphere, (b) Silica aerogel, (c) SC5, (d) SC10 and (e) SC15.

Fig. 8 (a-e) displays the particle size distribution of as obtained cenosphere and silica aerogel, and silica-cenosphere aerogels calcined at 1200°C. Table 2 gives diameter of these materials. The particle size and distribution curve of cenosphere powder is shown in Fig. 8.a. The major particle size distribution of cenosphere powder was between 20 and 300 μm. The shell thickness of cenosphere was reported to 1 to 18 μm [9]. The cenosphere typically has higher particle

size than the other prepared aerogel samples. The particle size and distribution curve of the as-prepared silica aerogel is shown in Fig. 8.b. Its median diameter was 27.15 μm .

SC5 aerogel (Fig. 8.c) had 14.65 μm median diameter and the maximum and minimum particle sizes of silica and SC5 aerogels were found to be nearly identical, but the shift in D50 was towards lower particle size. Fig. 8.d and Fig. 8.e shows particle size and distribution curve of SC10 and SC15 aerogel composites respectively. Both have closer median diameter (9.90 μm for SC10 and 8.48 μm for SC15) but D90 was reduced when the cenosphere content increased in silica aerogel.

Table 2. Diameter on cumulative % of Cenosphere, Silica Aerogel and Silica-Cenosphere Aerogels.

Material	Diameter on Cumulative %		
	D10(μm)	D50(μm)	D90(μm)
Cenosphere	21.31	72.23	156.08
Silica Aerogel	7.84	27.14	83.36
SC5	6.03	14.65	95.58
SC10	4.57	9.90	57.39
SC15	2.98	8.48	39.58

The particle size of silica-cenosphere aerogels decreased with increase in cenosphere content. The parameters like starting precursor materials, the synthesis method, the kind of heating pathway, and the temperature used influences the particle size and distribution.

Table 3 lists the surface area, pore volume, and pore diameter of as obtained cenosphere and silica aerogel and silica-cenosphere aerogels that were calcined at 1200 $^{\circ}\text{C}$. The specific surface area and pore volume of the silica-cenosphere aerogel were higher than silica aerogel and the values increased with increase in cenosphere weight percentages. Shrinkage is the most noticeable physical modification that takes place when an amorphous gel is heated above room temperature [6]. Because of the presence of cenosphere, silica aerogel shrank less at high temperatures, increasing its specific surface area and pore volume. Cenosphere addition to the prepared aerogels also resulted in an increase in pore diameter, however their pore diameters were lesser than that of cenosphere and silica aerogel.

Table 3. Surface area, pore volume and pore diameter of cenosphere, silica aerogel and silica-cenosphere aerogels.

Materials	Specific Surface area (m^2/g)	Pore Volume $\times 10^{-3}$ (cm^3/g)	Pore diameter (nm)
Cenosphere	6.6237	7.033	223
Silica aerogel	8.6878	13.612	230
SC5	13.8401	26.813	202
SC10	18.8272	31.724	209
SC15	23.7903	36.603	215

Fig. 9 displays the nitrogen adsorption isotherm linear plot against relative pressure (p/p°) of as obtained cenosphere and silica aerogel and silica -cenosphere aerogels after being calcined at 1200 $^{\circ}\text{C}$. Type-II isotherm was obtained and it represents unrestricted monolayer-multilayer adsorption. It displays a type A hysteresis loop corresponding to cylindrical capillaries that are open on both ends [7].

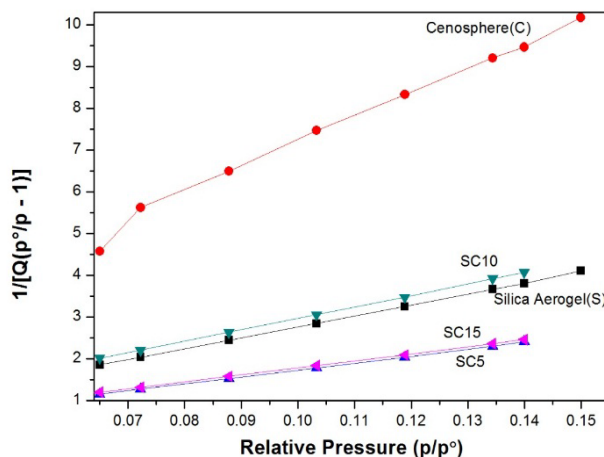


Fig. 9. Nitrogen adsorption isotherm linear plot.

Table 4 displays the physical properties of pellets of cenosphere, silica aerogel and silica-cenosphere aerogel.

Table 4. Physical properties of cenosphere, silica aerogel and silica-cenosphere aerogels.

Materials	True/Tap Density (g/cm ³)	HR	CI (%)	Flow character	Bulk Density (g/cm ³)	Apparent Porosity (%)	Water Absorption (%)
Cenosphere	0.99	1.08	8.08	Excellent	0.91	71.54	78.36
Silica aerogel	1.60	1.13	11.88	Good	1.41	32.67	23.16
SC5	1.57	1.13	11.47	Good	1.39	33.52	24.26
SC10	1.53	1.13	11.11	Good	1.36	38.11	27.97
SC15	1.45	1.12	11.12	Good	1.29	48.54	37.65

The powder flow behaviour during production determines whether a product succeeds or fails. HR and CI are the most important parameters commonly used to measure powder's flowability. The HR and CI ranges of the powders, which are 1.00-1.11 and 0-10, respectively, shows that the powder has outstanding flowability. The flowability of the HR and CI ranges of 1.12-1.18 and 10-16, respectively, is good, while the flow character of the HR and CI ranges of 1.19-1.25 and 16-20, respectively, is fair. There is extremely poor flow character in the HR and CI ranges of >1.60 and >38, respectively.

Due to its spherical shape, the cenosphere had the best flow characteristics of all the materials. Powder flow rate is influenced by the morphology, particle size and distribution. The flowability greatly improves as particle size increases. The samples of silica aerogel and silica-cenosphere aerogel composites had non-uniform particle distributions and a structure resembling popcorn, so they had less flowability than cenosphere.

Due to the hollow shape of the cenosphere and its extremely low density in comparison to silica aerogel, the density of silica-cenosphere aerogels decreased as cenosphere content increases. The porosity of silica aerogel values increased with the addition of cenosphere. The water absorption also increased when apparent porosity increased.

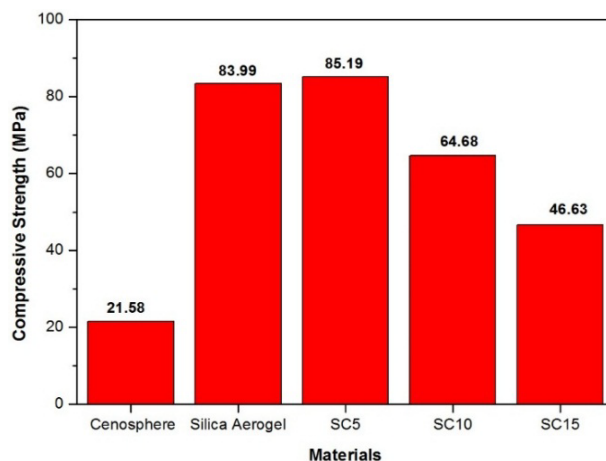


Fig. 10. Compressive strength of Cenosphere, Silica aerogel and silica-cenosphere aerogels.

The compressive strength of cenosphere, silica aerogel, cenosphere and silica – cenosphere aerogels are shown in Fig 10. The samples were prepared as pellets of 13 mm diameter with height of 26 mm (l/d ratio of 2 according to ASTM standard). Cenosphere showed lowest compressive strength value than all other samples because of the extremely low density (0.91 g/cm^3) and high porosity (71.54 %) of cenosphere. The compressive strength of SC5 was higher than silica aerogel and SC10 and SC15 aerogel composites. On introduction of 5wt% of cenosphere the variation in porosity and density was lesser. But the shell thickness of silica aerogel varied from below $50 \mu\text{m}$, and was mostly approximately $20 \pm 5 \mu\text{m}$ [9] and it is slightly stronger than cenosphere shell thickness ($1-18 \mu\text{m}$), so strength increased when cenosphere content was limited to 5wt%.

Further increase in cenosphere content led to considerable decrease in density and increase in porosity. When the content of cenosphere exceeded 5wt%, porosity increased significantly, agglomeration and micro-cracking tendency of cenospheres increased, which led to lower compressive strength in silica aerogel incorporated with more than 5wt% cenosphere. Since cenospheres are hollow spheres in nature, they are unable to transfer load to nearby particles. So, during the compression test, premature failure occurs [5]. Ozgur Kaya akmak et.al. [28] reported that the compressive strength of pure silica aerogel was 0.02 MPa and one of the reasons of the higher compressive strength can be usage of TEOS as a silica precursor because TEOS provide the control of porosity.

Xiurong Zhu et.al. [29] reported that the calculated Young's modulus of carbon aerogels was around 14.9 MPa and the maximum compressive strength of carbon aerogels were around 2.55 MPa.

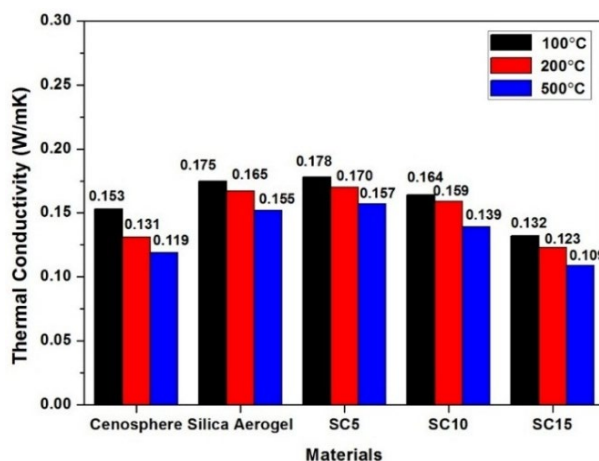


Fig. 11. Thermal conductivity of cenosphere, silica aerogel and silica-cenosphere aerogel composites at 100°C, 200°C and 500°C.

In Fig. 11, the thermal conductivity values of cenosphere, silica aerogel and silica-cenosphere aerogels are displayed. At temperatures of 100°C, 200°C, and 500°C, the thermal conductivity values of all the materials were measured. Due to the low density and high porosity of SC5, SC10 and SC15 by addition of cenosphere, all of the samples displayed a drop in thermal conductivity value with an increased in temperature. Ehsan Razaei et.al. [26] investigated that thermal conductivity of silica aerogel was 0.01349 W/mK with density of 140 kg/m³ at room temperature. When temperature increase thermal conduction of silica aerogel further increased till 100°C and then it is decreased when temperature increased further.

4. Conclusion

For the first time, a sol-gel method followed by subcritical drying was used to create silica-cenosphere aerogels. The effect of subcritical drying process on crystal structure, size and shape of particles, particle size distribution, specific surface area along with pore volume and pore diameter, physical properties and flowability of powders, compressive strength and thermal conductivity were evaluated. At calcination temperatures up to 1000°C, amorphous silica phase was identified in silica aerogel. At 1200°C, strong crystal integrity and a dominant α - cristobalite phase formed with a tetragonal structure. The amorphous silica (glass) phase and mixed oxide phases, such as mullite and quartz, were formed in cenosphere powder with orthorhombic and hexagonal structures, respectively. The amorphous silica phase containing the phases mullite, quartz, and cristobalite was also present in the silica-cenosphere aerogels. Increased cenosphere content in silica aerogel decreased the size of crystallites. In silica and silica-cenosphere aerogels, popcorn-like particle shape was observed by HR-SEM. Cenosphere powder had a perfect spherical shape, varied particle size and distributions, and microporous particle surface.

The highly intense peak that corresponds to Si-O-Si stretching vibrations with strong absorptions was found in all the samples in the FTIR spectrum. In SC15 aerogel, the Si-O-Al asymmetrical bend stretch was observed. The lowest particle size was found in SC15 with the addition of cenosphere and it was 8.48 μm , while 27.15 μm was the size of small particles in silica aerogel. Compared to silica aerogel and cenosphere, silica-cenosphere aerogel composites had a higher specific surface area, larger pore volume, and smaller pore diameter. SC15 had a higher specific surface area, pore volume, and smaller pore diameter than SC5 and SC10. Type II isotherm, which reflects unconstrained monolayer - multilayer adsorption, was observed. Cylindrical capillaries open at both ends were obtained along with a hysteresis loop classified as type A. Due to the incorporation of cenospheres in varying weight percentages, 8–18% variations in porosity values were observed in silica-cenosphere aerogels. Compared to silica-cenosphere aerogels, silica aerogel had a higher bulk density. Bulk density of the silica aerogel decreased from 1.41 to 1.29 g/cm³ by the addition of cenosphere.

Cenosphere had an outstanding flow behaviour and a bulk density of 0.91 g/cm³. Samples of silica and silica-cenosphere aerogels exhibited good flow behaviours. The porosity value was the only factor that had any influence on the compressive strength of the cenosphere and the prepared aerogel samples. The cenosphere sample has the lowest compressive strength value, 21.58 MPa, as a result of its extremely low density. SC15 had the lowest compressive strength, which was measured at 46.63 MPa, due to its highest porosity value of 48.54%. 97.36% silica and 1.51% alumina were present in the silica aerogel. When cenospheres were added, the alumina percentage increases with corresponding decreases in silica content. In SC15, it was found that silica decreased to 92.2% while alumina increased to 5.61%. The thermal conductivity of silica-cenosphere samples reduced from 0.178 W/mK to 0.109 W/mK with raising temperatures and cenosphere addition. At 500°C, silica aerogel and the cenosphere both reached their maximum thermal conductivities of 0.119 W/mK and 0.155 W/mK, respectively. Due to their reduced thermal conductivity values, the silica and silica-cenosphere aerogels are suitable for thermal insulation applications such as energy-efficient buildings, cold-chain transportation and aerospace engineering.

Acknowledgements

The authors would like to acknowledge the Anna University Chennai and Department of Ceramic Technology.

References

- [1] Saorise Dervin, Yvonne Lang, Tatiana Perova, Steven H. Hinder, Suresh C.Pillai, *Journal of Non-Crystalline Solids*, **465**, 31(2017); <https://doi.org/10.1016/j.jnoncrysol.2017.03.030>
- [2] C.A.Garcia-Gonzalez, M.C.Camino-Rey, M.Alnaief, C.Zetzl, I.Smirnova, *The Journal of Supercritical Fluids*, **66**, 297 (2012); <https://doi.org/10.1016/j.supflu.2012.02.026>
- [3] S.R.Venkatasubramanian, R.Manikandan, K.Abirami, V.Karthikeyan, Subhalakshmi S, *International Journal of Engineering Science Invention*, ISSN (Online): 2319-6734, ISSN (Print):2319-6726, 31(2017)
- [4] Tomasz Blaszczyński, Agnieszka Słosarczyk, Maciej Morawski, *Procedia Engineering*, **57**, 200 (2013); <https://doi.org/10.1016/j.proeng.2013.04.028>
- [5] Rajeev Kumar, D.P.Mandal, Anisha Chaudhary, Muhamed Shafeeq, Saroj Kumari, *Composite Part A: Applied Science and Manufacturing*, **112**, 475 (2018).
<https://doi.org/10.1016/j.compositesa.2018.07.003>
- [6] P.R.Aravind, P.Mukundan, P.Krishna Pillai, K.G.K Warriar, *Microporous and Mesoporous Materials*, **96** (1-3), 14 (2006); <https://doi.org/10.1016/j.micromeso.2006.06.014>
- [7] Srinivasulu Kasala and Manisha Vidyavathy Sudandara Doss, *Transactions of the Indian Ceramic Society*, **78** (1), 13(2019); <https://doi.org/10.1080/0371750X.2019.1566024>
- [8] Srinivasulu K, Manisha Vidyavathy S, *Journal of Ceramic Processing Research*, **20**(1), 8(2019). <https://doi.org/10.36410/jcpr.2019.20.1.8>
- [9] Navid Ranjbar, Carsten Kuenzel, *Cenosphere: Fuel*, **207**, 1(2017);
<https://doi.org/10.1016/j.fuel.2017.06.059>
- [10] N. Hüsing, U. Schubert, *Angewandte Chemie (A Journal of the German Chemical Society)*, **37**, 22(1998); [https://doi.org/10.1002/\(SICI\)1521-3773\(19980202\)37:1/2<22::AID-ANIE22>3.0.CO;2-I](https://doi.org/10.1002/(SICI)1521-3773(19980202)37:1/2<22::AID-ANIE22>3.0.CO;2-I)
- [11] A.C. Pierre, G.M. Pajonk, *Journal of Chemical Reviews*, **102**(11), 4243 (2002),
<https://doi.org/10.1021/cr0101306>
- [12] R. Baetens, B.P. Jelle, A. Gustavsen, *Energy and Buildings*, **43**(4), 761(2011),
<https://doi.org/10.1016/j.enbuild.2010.12.012>
- [13] M. Koebel, A. Rigacci, P. Achard, *Journal of Sol-Gel Science and Technology*, **63**, 315 (2012); <https://doi.org/10.1007/s10971-012-2792-9>
- [14] E. Cuce, P.M. Cuce, C.J. Wood, S.B. Riffat, *Renewable and Sustainable Energy Reviews*, **34**, 273(2014); <https://doi.org/10.1016/j.rser.2014.03.017>
- [15] Y. Yu, X. Wu, J. Fang, *Journal of Materials*, **50**, 5115(2015), <https://doi.org/10.1007/s10853-015-9034-9>
- [16] Z. Wu, L. Zhang, J. Li, X. Zhao, C. Yang, *RSC Advances*, **8**, 5695(2018);
<https://doi.org/10.1039/C7RA13165H>
- [17] Abolghasemi Mahani, S. Motahari, A. Mohebbi, *Marine Pollution Bulletin*, **129**(2), 438(2018); <https://doi.org/10.1016/j.marpolbul.2017.10.012>
- [18] J. He, H. Zhao, X. Li, D. Su, F. Zhang, H. Ji, R. Liu, *Journal of Hazardous Materials*, **346**, 199(2018); <https://doi.org/10.1016/j.jhazmat.2017.12.045>
- [19] D.B. Mahadik, Kyu-Yeon Lee, R.V. Ghorpade, Hyung-Ho Park, *Scientific Reports*, **8**, 16783(2018); <https://doi.org/10.1038/s41598-018-34997-1>
- [20] G.M. Pajonk, *Applied Catalysis*, **72**(2), 217(1991); [https://doi.org/10.1016/0166-9834\(91\)85054-Y](https://doi.org/10.1016/0166-9834(91)85054-Y)
- [21] Y. Zhao, Y. Liang, X. Zhao, Q. Jia, H. Li, *Progress in Natural Science: Materials International*, **21**(4), 330(2011); [https://doi.org/10.1016/S1002-0071\(12\)60065-3](https://doi.org/10.1016/S1002-0071(12)60065-3)
- [22] J.P. Randall, M.A.B. Meador, S.C. Jana, *ACS Applied Material Interfaces*, **3**(3), 613(2011);
<https://doi.org/10.1021/am200007n>

- [23] N. Bheekhun, Abd.R. Abu Talib, M.R. Hassan, *Advances in Materials Science and Engineering*, **2013**, 1(2013); <https://doi.org/10.1155/2013/406065>
- [24] Xiaoman Xiong¹, Tao Yang¹, Rajesh Mishra¹, Hiroyuki Kanai² and Jiri Militky¹, *Journal of Industrial Textiles*, **47**(8), 1998 (2018); <https://doi.org/10.1177/1528083717716167>
- [25] Agnieszka Slosarczyk, Andrii Vashchuk and Łukasz Klapiszewski, *MDPI(Polymers)*, **14**(7), 1456(2022); <https://doi.org/10.3390/polym14071456>
- [26] Ehsan Rezaei, Jafarsadegh Moghaddas, *Advanced Materials Letters*, **7**(4), 296(2016); <https://doi.org/10.5185/amlett.2016.6178>
- [27] Jyoti Guruv, In-Keun Jung, Hyung-Ho Park, Eul Son Kang and Digamber Y.Nadargi, *Journal of Nanomaterials*, Article ID 409310, 11 pages (2010); <https://doi.org/10.1155/2010/409310>
- [28] X.Han, K.Hassan, A.Harvey, D.Kulijer, A.Oila, M.Humt, L.Siller, *Advanced Materials*, **30**, 1706294(2018); <https://doi.org/10.1002/adma.201706294>
- [29] Xiurong Zhu, Lousia J. Hope-Weeks, Roya Baghi, Vanessa R. Charles, Yi Yu, Lingwei Zhu, Xinghua Wang, Dongbo Li & Xianghua Zeng, *Journal of Porous Materials*, **29**, 1279(2022); <http://doi.org/10.1007/s10934-022-01254-w>